Indian J. Phys. 76A (4), 325-342 (2002)

IJP A
-- an international journal

Physical behaviour and theoretical understanding of nanowires

Shalinee Chikara, Ratan Lal and S K Joshi*

Theory Group, National Physical Laboratory,
K. S. Krishnan Road, New Delhi-110 012, India

E-mail : skjoshi@csnpl.ren.nic.in

Received 20 May 2002, accepted 22 May 2002

Abstract . Existing and ongoing studies on nanowires present a scenario of rapid developments and we review here main physical properties of these systems along with the theoretical methods relevant to their understanding. Conductance quantization in the ballistic regime has been described under various conditions. Resistivity of the nanowires of length longer than the transport mean free path is described for various materials. Coulomb drag and superconducting behaviour of nanowires are presented. Optical behaviour, Raman spectra and magnetic behaviour of nanowires are also discussed. An illustration of electronic subbands formation is given by using a tight binding approach. Standard theoretical methods, namely Landauer approach and Luttinger liquid approach which are applicable to one-dimensional systems are reviewed in brief. For thick nanowires that cannot be considered one-dimensional there is a need for other theoretical methods. A survey is presented of a number of methods employed by different workers for investigating various physical properties of the nanowires.

Keywords . Nanowires, electronic structure, transport behavior

PACS Nos. 73.22.-f, 73.23.-b, 73.63.-b

PLAN OF THE ARTICLE

Corresponding Author : Also at Jawaharlal Nehru Centre for Advanced Scientific Research, Jakkur P. O., Bangalore-560 064, India.

1. Introduction

Consider a system with dimensions L_x, L_y and L_z along the x, y and z-axes respectively in the space. A wire will correspond to the situation where $L_x >> L_y, L_z$. While L_x is supposed to denote the length of the wire, L_y and L_z define its cross-sectional dimensions. The shape of the cross-section of the wire may be of many types like rectangular (breadth = L_y, width = L_z), elliptical (major axis = L_y, minor axis = L_z) or circular (diameter = $L_y = L_z$). When L_y and L_z are of the order of 100 nanometer or less, the wire is called 'nanowire'. A wire having L_y and L_z of the order of 100 microns or more will be a 'macrowire' or bulk wire.

In recent years nanostructured materials have drawn tremendous amount of attention due to their new promising applications in the electrical, optical, and magnetic device fields [1-4]. The devices based on nonowires show high quantum efficiency as compared to the devices on macrowires [5]. For example, single-walled carbon nanotubes have been used as building blocks to fabricate room-temperature field-effect transistors [6-8], diodes [9, 10], and an inverter [11], which represents a key component for a logic circuit. Semiconductor nanowires have also been used as building blocks for assembling a range of nanodevices including field-effect transistors [12, 13], p-n diodes [13, 14], bipolar junction transistors, and complementary inverters [14]. Moreover, silicon on-insulator quantum wire has been fabricated and from this a single-electron transistor has been developed [15-17]. The single-electron transistor has been applied to logic circuits such as inverter [18] and exclusive-OR gates [19]. Studies are also going on in the area of optoelectronic devices based on InAs/InP self-assembled nanowires in the wavelength range 1.3–1.55 μm [22-23]. Apart from their use in devices, nanowires can also function as interconnection wires in nanoelectronic devices [5].

When a nanowire is used like a device, it is connected at both the ends by three dimensional (3D) leads [24]. In fact the 'nanowire' sample is considered only a part of a larger system containing 'ideal leads' that connects the 'reservoir' with the sample. The 'reservoirs' are characterized by their chemical potentials. In a typical experiment (like electric transport) one connects the 'nanowire' sample to charge 'reservoir'. This situation is shown schematically in Figure 1 where we have considered a 'nanowire sample delimited by $[-L_x/2, L_x/2]$ in x-direction. The y-and z- directions are assumed to be perpendicular to the length of the wire. In Figure 1 we show the nanowire and ideal leads only in x-y plane. The left (right) reservoir injects bare right (left) going electrons with a well defined electrochemical potential μ_1 (μ_2) [25]. Because of the confinement of the electrons in a nanowire along two directions, the properties of these wires become very sensitive to their

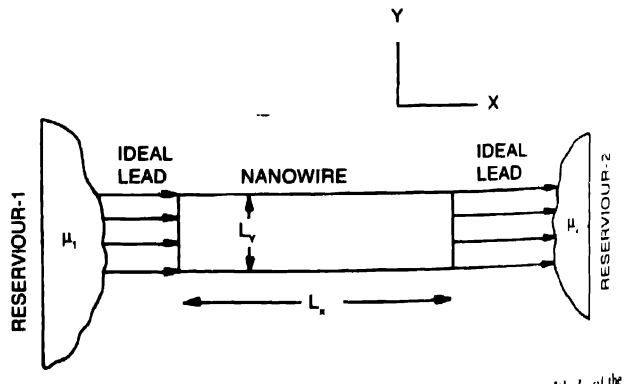

Figure 1. A nanowire of length L_x and width L_y is shown. Breadth L_z of the nanowire is not shown as the figure corresponds to X–Y plane only. The wire is connected to reservoirs of chemical potentials μ_1 and μ_2 through ideal leads. The ideal leads provide transport channels shown by arrow

shape and size. Experimental and/or theoretical investigations have shown that optical, electrical, magnetic, superconducting and many other properties of the nanowires show such features, which are hitherto unknown in the macroworld. It must however be noted that in the experimental measurements care should be taken to ensure that it is the (quasi-) one dimensional physics of the nanowire rather than the three-dimensional physics of the 'leads' which is being probed. This will be the case provided the wire is larger than the thermal coherence length [26]

$$L_T = \frac{\hbar v_F}{k_B T}. \tag{1}$$

Here, $\hbar$ is the Plancks constant divided by 2π, v_F is Fermi velocity, k_B is the Boltzmann constant and T is the temperature of the wire. In a GaAS nanowire of length L_x = 1 μm and of electron density of one electron per 10 nm eq. (1) will need $T \geq 10$ mK for $L_T \leq L_x$ [26]. Thus for a micron length GaAs nanowire experiment should be performed above 10 mK for analyzing one dimensional physical phenomenon.

In this article, we present a survey of the general behaviour of the physical properties of nanowires and also provide a brief account of the theoretical methods developed for understanding the physical behaviour of these systems. Because we only wish to convey a broad picture of the field rather than exhaustive account, we had to choose only a few references. Our apologies to authors whose work we could not include in this article. In Section 2 we describe the types of nanowires from different angles. Nearly all the properties we discuss depends on electrons, we therefore present formation of electronic subbands in Section 3. Various physical properties of the nanowires are presented in Section 4, while theoretical methods are described in Section 5.

2. Types of nanowires

In a broad sense we can classify the nanowires in two different ways: (i) On the basis of the type of the material used in the fabrication or synthesis of the wire, and (ii) On the basis of the method of preparation of the wire.

2.1 *Material-based classification*

We have four types of nanowires (i) metallic nanowires (ii) semiconducting nanowires (iii) semimetallic nanowires and (iv) carbon-based nanowires.

2.1.1. *Metallic nanowires*

Nanowires of metallic materials like wires of Na, Cu and Al [27-29] come in this category. In such wires, the effective mass of the electrons, m^*, will be nearly equal to the bare mass of electron, m_0.

Computer simulation on Al and Pb nanowires suggest that ultrathin wires of these metals should develop exotic, non-crystalline stable atomic structures once their diameter decreases below a critical size [30, 31]. The new structures, whose details depend upon the material and wire thickness, may be dominated by icosahedral packing. Gulseren, Ercolessi and Tosatti [30, 31] proposed to name such wires 'weird' wires. A possible reason for the wire structure to switch from crystalline structure to weird structure is the smaller relative surface/bulk ratio in the wires. It may be noted that for a nanowire $L_y << L_x$. So, the surface area of a cylindrical nanowire (of diameter $L_y = L_z$) will be $\frac{1}{2}\pi L_y^2 + \pi L_y L_x \approx \pi L_y L_x$ contrary to the area $\frac{3}{2}\pi L_x^2$ of a 3D cylinder. So, the relative surface/bulk ratio will be $12/L_y$ for a nanowire as compared to $18/L_y$ for a 3D system. A synthesis of weird wire is yet to be reported. Very recently, Wang and coworkers [32] have used tight-binding approach for the study of ultrathin titanium nanowires. They found that such nanowires show helical multiwalled cylindrical structures with pentagonal packing in very thin wires and hexagonal packing in thinner ones.

2.1.2. *Semiconducting nanowires*

Nanowires based on semiconducting materials like Si, Ge and InSb belong to this group [33-36]. The effective mass of an electron in such nanowires is relatively much smaller than the free electron mass m_0. In fact, m^* will be of the order of $m_0/100$ or $m_0/10$. (see Table 1). While nanowires of semiconducting materials are expected to show semiconducting behaviour, Landman and coworkers [33] have shown by computer simulation of Si nanowires that when the length of the wire is short (~ 0.6 nm) the wire will show metallic behaviour. Silicon and silicon-based nanowires [37-39], Ge nanowires [34, 37], SiC nanowires [40-42] and Si_3N_4 nanowires [43] all have a uniform crystalline core with an amorphous oxide outer layer [44]. However, synthesis of Ge nanowires by Gu and coworkers [35] has shown that Ge nanowires can be synthesized in the single crystalline form also.

Table 1. Effective mass of electrons, m^*, in some of the nanowire materials m_0 is the mass of the bare electron

Material	m^*/m_0	Reference
GaAs	0.066	64
InGaAs	0.041	64
InSb	0.015	36
CdTe	0.091	65

2.1.3. *Semi-metallic nanowires*

Bismuth and antimony are semimetals. Bi nanowires exist in the crystalline form [45, 46]. An interesting feature of the Bi nanowires is that their structure is not affected by alloying with Sb upto 15 at. % [47]. On the other hand, the structure of antimony nanowires is different from bismuth in that the antimony nanowires exist in a form, which is combination of both the crystalline and amorphous phases [48]. The maximum

ratio of the crystalline to amorphous form in antimony wires is obtained by annealing at 150 C [48, 49].

2.1.4. Carbon-based nanowires

Carbon exists in three forms-diamond, graphite and fullerenes. Graphite needles having diameters of usually 2 nm to 30 nm and length ~ 1 μm are carbon-based nanowires. These are essentially rolled up sheet of carbon hexagons. As these are hollow from inside, the carbon nanowires are usually called carbon nanotubes [1]. These nanotubes can be either a metal or semiconductor depending on their diameters and helical arrangement of carbon atoms. The helical arrangement about the tube axis is specified as follows. Let $a/\sqrt{3}$ be the nearest-neighbor C-C distance in a carbon hexagon of a graphite sheet. Then $\boldsymbol{a} = a\boldsymbol{i}$ and $\boldsymbol{b} = \left(-\boldsymbol{i} + \sqrt{3}\,\boldsymbol{j}\right)a/2$ will denote the primitive translational vectors. Here, $\boldsymbol{i}$ ($\boldsymbol{j}$) is a unit vector along the $X(Y)$-axis of Cartesian coordinates. A given vector $\boldsymbol{R}$ in the graphite sheet will be given by $\boldsymbol{R} = n_a\boldsymbol{a} + n_b\boldsymbol{b}$. The helicity of the carbon nanotube is denoted by (n_a, n_b). When $n_b = 0$, we have the commonly called 'zigzag' nanotube, while when $n_a = 2n_b$, it will be an 'armchair' nanotube [1].

2.2. Fabrication-based classification

2.2.1. Nanotubes

Nanotubes are normally formed by arc discharge, laser ablation and catalytic decomposition of reacting gases. Nanotubes include carbon nanotubes [1], BN nanotubes [50] NbS_2 nanotubes [51, 52], TaS_2 nanotubes [51, 52] and $Na_2V_3O_7$ nanotubes [53, 54]. As the name implies these nanowires are hollow from inside. The nanotubes have a well defined structure

2.2.2. Cast-in-tubes and tube-coated nanowires

Cast-in-tubes are fabricated by filling hollow channel templates of carbon nanotubes or of porous materials like anodic alumina. For example, carbon nanotubes are used in this way to produce Cr [55], Pb [56] and GaN [57, 58] nanowires. The surface energy of the cast-in-tube nanowires is expected to be low because there are no dangling bonds on their surface. Nanowires can also be fabricated by coating the outside of nanotubes. The difficulty with such wires is that their diameter is not uniform [45]. However, Bezryadin and coworkers [59] have fabricated MoGe nanowires of thickness of order of 10 nm by sputtering a superconducting alloy of amorphous $Mo_{79}Ge_{21}$ over a freestanding carbon nanotube.

2.2.3. Island-shaped nanowires

Such nanowires are synthesized on a substrate surface using various techniques such as molecular beam epitaxy [60], electron beam lithography [61] and scanning tunneling microscope pattern writing [62]. The surface energy of the island-shaped nanowires should be low because there is a large interface area between the island and the substrate.

2.2.4. Free standing nanowires

This group of nanowires comprises of freestanding nanowires [32], which have been synthesized by laser ablation. Such wires have relatively very large surface energy especially for sp-bonded covalent materials, and it is very difficult to synthesize them by other methods. In fact, the high surface energy gives rise to structural instability, thereby putting constraints on the minimum value of the diameter of the free standing nanowire [34].

3. Formation of electronic subbands

Before describing the physical behaviour of nanowires it will be advantageous to have knowledge of the energy levels in these systems. Because of the confinement of the electronic wave function along the y and z- directions the energy levels of the nanowires will show subbands. Kramer and Masek [24, 63] have worked out a systematic study of energy levels in nanowire systems within a tight-binding approach. They considered a nanowire made of a square lattice (with lattice constant a) such that

$$L_z = Na$$

and

$$L_y = Ma.$$

This simple two-dimensional model describes the essential physics of energy levels of a nanowire with N as the number of sites along the wire length and M as the number of sites in the direction perpendicular to the wire axis. Since for a nanowire $l \ll L_x$, it is clear from eqs. (2) and (3) that $M \ll N$. In fact, from a practical viewpoint, it may be assumed that $N \to \infty$, while M is of the order of 10–100.

In a tight-binding approach [63], the Hamiltonian of the nanowire may be written in the form

$$H = \sum_{j=1}^{N}\sum_{m=1}^{M-1}|jm\rangle\langle j, m+1| + V\sum_{j=1}^{N-1}\sum_{m=1}^{M}|jm\rangle\langle j+1, m| + H.C. \quad (4)$$

Here, (j, m) denote the site index ($j = 1, 2 \ldots\ldots M$). The lattice constant is taken to be unity so that $L_x = N$ and $L_y = M$. The hopping matrix element between nearest-neighbors in the m direction (y-direction) is taken to be the unit of the energy. V is the hopping matrix element between nearest neighbors in the j direction (x-direction). Periodic boundary conditions are taken in the j-direction, which is possible because length of the nanowire is large ($N \to \infty$).

The Schrödinger equation corresponding to the Hamiltonian H (eq. (4)) may be written as

$$c_{j,m+1} + c_{j,m-1} + V\left(c_{j+1,m} + c_{j-1,m}\right) = Ec_{jm}, \quad (5$$

where c_{jm} is the component of the eigenfunction at the (j, m) site and E is the eigenenergy. Because of the periodicity of the atomic arrangement in the j-direction, we may take $c_{mj} = c_m \exp(ikj)$ with $-\pi < k \leq \pi$. When it is so, eq. (5) will be reduced to

$$c_{m+1} + c_{m-1} + 2Vc_m \cos k = Ec_m . \tag{6}$$

This is formally the same as the expression obtained for an isolated system of length M in the m-direction, except that an additional m-dependent diagonal term occurs. Let $c_m^{\nu k}$ ($\nu = 1, 2, \ldots M$) denote the solution of the M-dimensional system of equations represented by eq. (6) with the corresponding eigenvalue

$$E_{\nu k} = E_\nu + 2V \cos k \tag{7}$$

and wave function

$$|\Psi_{\nu k}\rangle = N^{-\frac{1}{2}} \sum_{m=1}^{M} \sum_{j=1}^{N} c_m^{\mu k} e^{ikj} |jm\rangle . \tag{8}$$

The orthogonality of the eigenstates implies

$$\sum_{m}^{M} \left(c_m^{\nu k}\right)^* c_m^{\nu' k} = \delta_{\nu\nu'} . \tag{9}$$

In eq. (7), E_ν is the energy corresponding to the transverse (m-direction) states of the nanowire. In Figure 2, values of E_ν are shown for different ν for $M = 10$. These values are based on Ref. [63]. The full energy $E_{\nu k}$ is plotted in Figure 3 [63]. It is clear from the figure that the energy spectrum consists of well separated quasi 1D energy bands. The reason for this lies in the geometrical constraint on the motion of the electrons perpendicular to the x-direction.

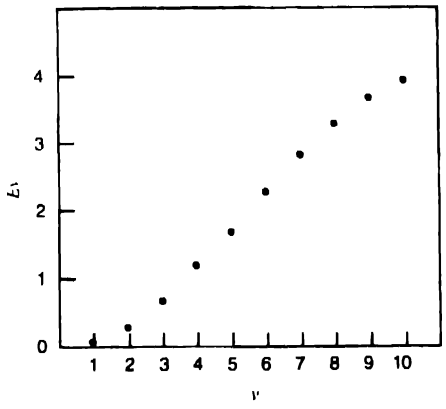

Figure 2. Variation of the Energy E_ν of the transverse motion in a nanowire modeled by a $N \times M$ lattice structure with $N \to \infty$ and $M = 10$. The quantum number ν distinguishes the ten quantum states. Values of E_ν are based on Figure1 of Ref. [63].

From the viewpoint of existence of quantum effects, it is required that the subband splitting be large. One of the parameter, which controls the subband splitting is the effective mass, m^*, of the electrons. In Table I we present effective mass of electrons for some of the nanowire materials [36, 64, 65]. It is clear that out of the systems presented in Table I, InSb corresponds to the least effective mass of electron, and so is most suitable for the appearance of the quantum effects. In fact, InSb nanowires are indeed found to show a 1D behaviour [36]. In the ridge-type InGaAs nanowires (of diameter 300 nm) the subband splitting as large as 7.4 meV are observed [66].

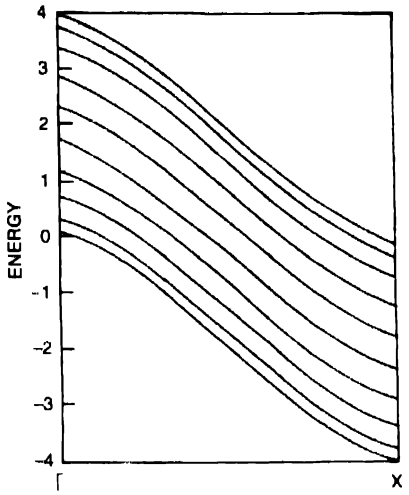

Figure 3. Electronic subbands for a nanowire specified in Figure 1 of Ref. [63] and replotted by enlarging the momentum axis ΓX. The different subbands corresponds to different ν, the lowest one corresponding to $\nu = 1$.

4. Physical behaviour of nanowires

4.1. Conductance under ballistic transport

The conductance of nanowires depends upon the conditions, which describe the status of carriers (*i.e.* electrons). In the simplest possible case one considers measurements on a nanowire having noninteracting electrons. Other possible cases include : nanowire under a high magnetic field, nanowires with interacting electrons and disordered nanowires. The conductance will, in general, be different in different cases. Apart from this description of carriers and conditions that prevail during measurement the conductance also depends upon the length of the wire. Of particular interest is the case when the length of the nanowire is less than the transport mean free path. In this case, the nature of the transport will be ballistic, and will lead to infinite conductance. But, because of the fact that the nanowire is connected on its two sides by leads, there will be lead-nanowire contacts in the circuit. These contacts make the conductance finite. In this section, we shall consider conductance of only such nanowires, which are shorter than the transport mean free path. Conductance for the lengths of wires greater than the mean free path will be described in the next section (Sec. 4.2).

4.1.1. Noninteracting electrons without external field

Conductance has been measured in different kinds of nanowires of metals (Au, Al, Pb, Na, Hg and Sb), of amorphous metals (Co-Fe-Si-B), of semi-metal (Bi) and of ceramics (La-Sr-MnO_3)

[67]. It has been found that the conductance is quantized in steps of

$$G_0 = 2e^2/h, \tag{10}$$

(c.f. Figure 4). The first reports about quantization of conductance were made by van Wees and coworkers [68] and Wharam and coworkers [69] in the two-dimensional gas of a GaAs-AlGaAs heterostructure. The origin of the conductance quantization lies in the ballistic transport through a nanocontact region between the paramagnetic lead wires. In the case of ferromagnetic leads the situation is more complicated and still under debate [63]. Although it is known that single experiments on Ni nanowire do show conductance quantization, there is still controversy about the structure of conductance, which has been reported to be almost featureless [70, 71]. This is in contrast to the case of Fe nanowires whose conductance shows pronounced peaks [70].

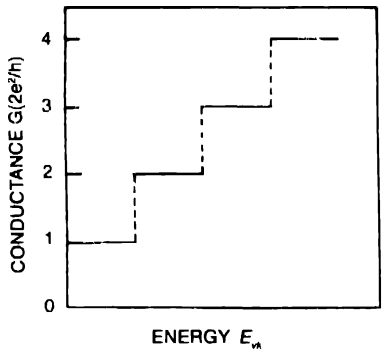

Figure 4. Variation of conductance G with the energy due to the ballistic transport through a nanowire connected to paramagnetic lead wires on both the sides. The energy axis shows the filling of the subbands.

4.1.2. Carbon nanotubes

Conductance quantization is also shown by metallic ('arm chair') carbon nanotubes [1]. An 'arm chair' carbon nanotube is a metallic nanowire with two linear electronic energy bands that cross at the Fermi energy E_F. Because of this the conductance of defectless carbon nanotubes will be quantized in units of $2G_0 = 4e^2/h$ [72-74], contrary to the conductance quantization in units of G_0 in other types of nanowires. Defects reduce the conductance by a quantum unit G_0 [75].

4.1.3. Spinless electrons in one-dimensional constrictions in GaAs/$Al_xGa_{1-x}As$ heterostructures

In the case where the nanowire system is kept in a strong magnetic field, spin of the electrons will not be so relevant, and so the nanowire will behave as a system of spinless electrons [26]. In such systems conductance will be quantized in units of $G_0/2 = e^2/h$. Thomas and coworkers [76] have measured conductance of one-dimensional constrictions defined by split gates in high quality GaAs/$Al_{0.33}Ga_{0.67}As$ heterostructures by applying a magnetic field of 16T. This field was found strong enough to lift the spin degeneracy of the 1D subbands giving conductance plateaus quantized in units of $G_0/2$.

4.1.4. One-dimensional constrictions in GaAs/$Al_xGa_{1-x}As$ heterostructures in variable magnetic field

In another experiment on one-dimensional constrictions defined in high mobility two-dimensional electron gas, formed at modulation-doped GaAs/$Al_{0.33}Ga_{0.67}As$ heterostructure grown on a (100) GaAs substrate, Thomas and coworkers [77] have found upto 26 quantized ballistic plateaus in zero magnetic field. Apart from this they have seen a structure in the rising edge of the conductance *versus* energy curve starting at around $0.7\,G_0$. This structure merges with the first conductance plateau with increasing energy. When one increases the in-plane magnetic field, the structure moves down and eventually merges with a new conductance plateau at $G_0/2$ in very high fields [77]. Efforts to explain this feature of the conductance of the clean and nearly straight nanowires have been made by many authors [78-80]. These authors have used ideas like involvement of spin polarized subbands [78], conductance suppression in a Luttinger liquid with repulsive interaction and disorder [79] and local spin-polarized density functional theory. Very recently, Rejec and coworkers [80, 81] have suggested an interesting explanation of the behaviour of the conductance threshold. They have shown that quantum wires with weak longitudinal confinement, or open quantum dots can give rise to spin-dependent, Coulomb blockade resonances when a single electron is bound in the confined region. The emergence of a specific structure at $G_{int} \sim G_0/4$ and $G_{int} \sim 3G_0/4$ is a consequence of the singlet and triplet nature of the resonances, with a probability ratio 1:3 for singlet and triplet scattering and as such is a universal effect.

4.1.5. Reduction of quantization step

In nanowires where interaction between the electrons is important, it is predicted [26] that the conductance will be renormalized to

$$G_{int} = \eta G_0, \tag{11}$$

where $\eta > 1$ corresponds to attractive interaction among electrons, while $\eta < 1$ corresponds to repulsive interaction. As is obvious from eq. (11), $\eta = 1$ corresponds to the noninteracting case.

In 1995, Tarucha and coworkers [82] performed conductance measurements on GaAs nanowires of length $L_x = 2 - 10\,\mu m$ and interpreted their measurements using a modified Luttinger liquid theory of Ogata and Fukuyama [83] that takes into account the scattering due to disorder. They estimated η to lie from 0.65 to 0.7. This implies that there exists a significant interaction among the electrons of these nanowires, and that the conductance is reduced by 30% in the ballistic limit. But the reduction of the conductance observed by Tarucha and coworkers is only a few percent, suggesting $\eta \approx 1$. This led Maslov and Stone [84] to argue that the conductance of a quantum wire is G_0 regardless of the interactions amongst electrons in the wire. This is because the finite conductance of a ballistic wire is due to a contact

resistance and comes entirely from processes that take place outside the wire, where the electrons follow the Fermi liquid description.

4.1.6 *Quantization of thermal conductance*

Till now we have considered the electrical conductance in the ballistic regime of nanowires. Quantization has also been observed recently in the thermal conductance [85]. Schwab and coworkers [85] have fabricated a phonon cavity in the form of a wire from a 60 nm thick SiN membrane by electron beam lithography and pattern transfer techniques. The SiN membrane is used in the fabrication of phonon wires because its structural layer provides a homogeneous effective medium for the long wavelength phonons of relevance to the ballistic propagation of phonons at low temperatures.

The universal quantum of thermal conductance observed by Schwab and coworkers [85] at low temperature is given by

$$G_0^{th} = \pi^2 k_B^2 T / 3h . \tag{12}$$

This quantum of thermal conductance represents the maximum possible value of energy transported per phonon mode. It does not depend on particle statistics-but is the universal value for fermions, bosons and anyons.

4.1.7 *Comparison of electrical and thermal conductance*

Electrical and thermal conductance quantizations are manifestly different in a number of ways. Two of the most obvious differences are :

1. The factor of T in eq. (12), reflects the fact that the quantity transported is Thermal energy. In the case of electronic conduction, the corresponding quantity is the electronic charge, and the electrical conduction quantum per spin-degenerate band is temperature independent, $G = G_0$ (cf. eq. (10)).
2. In electrial conductance a series of conductance steps are observed (Figure 4). In such measurements, chemical potential and temperature can be controlled separately. At a fixed low temperature, the Fermi energy can be changed by changing electron density, which allows us to sweep sequentially the different electron states of the nanowire. With phonons, one can change only temperature. In phonons the Bose distribution smears out all features except at very lwo temperatures when the lowest energy phonons alone contribute [86].

4.2 *Resistivity*

In the previous section we considered conductance of such nanowires whose length is less than the transport mean free path In this section we consider conductance of nanowires of lengths larger than the transport mean free path. Rather than conductance we shall consider resistivity ρ, which is related with the conductance by

$$\rho = A / GL_x \tag{13}$$

where A is the cross sectional area ($A = \pi L_y^2 / 4$ for circular cross section, while $A = L_y L_z$ for rectangular cross section).

We consider the behavior of resistivity separately for the follwing four cases : (i) Metallic nanowires, (ii) Nanowires made of semimetallic materials, (iii) Nanowires made of semiconducting materials, and (iv) Nanowires based on carbon nanotubes.

4.2.1. *Metallic nanowires*

The electrical resistivity of metallic wires of length much larger than the transport mean free path is governed by diffusive transport and is independent of the length of the wire. The intermediate regime, where a nanowire has dimensions of the order of the mean free path (l) is considered by Durkan and Welland [29]. They have carried out a study of the width (L_y) dependence of the resistivity of the polycrystalline gold (Au) nanowires. It has been found that below the nanowire thickness $L_y \approx 60$ nm, the resistivity of the wire starts to increase with decrease in wire thickness (Figure 5). Durken and Welland argue that the experimental results of the increase of ρ with decreasing

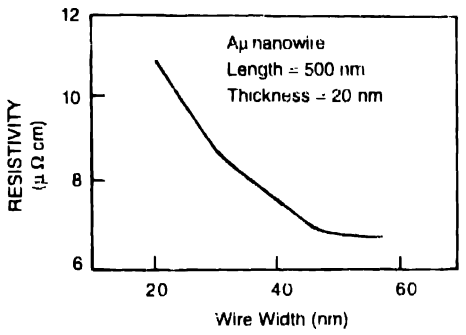

Figure 5. Schematic variation of resistivity with the thickness of Au nanowires This figure is based on the work of Durkan and Welland (Ref. [29]).

L_y can be explained by a combination of the surface and grain-boundary scattering mechanisms. In fact, Durkan and Welland have used a modified Mayadas-Shatzkes approach [87, 88], incorporating the variation of mean grain size with wire dimensions. According to the Mayadas-Shatzkes model, the resistivity of the nanowire is given by

$$\rho = \rho_0 \left[1 - \frac{3\alpha}{2} + 3\alpha^2 + 3\alpha^2 \ln\left(1 + \frac{1}{\alpha} \right) \right]^{-1} \tag{14}$$

Here, $\alpha = lR / D_{eff} (1 - R)$ with l as the electronic mean free path, D_{eff} as the average distance between grain boundaries, and R as the grain-boundary reflection coefficient.

4.2.2. Semimetallic nanowires

Barati and coworkers [48] synthesized antimony (Sb) nanowire arrays of different diameter L_y of 20 nm, 100 nm and 200 nm. They measured resistance of this array and found several interesting results . (i) The resistance of all the Sb nanowires is characterized by an exponential behavior e^{E/k_BT} (Figure 6) where E is the characteristic excitation energy. (ii) In the case of the 200 nm diameter nanowire, the resistivity has two values of excitation energies, 60 meV at high temperatures and 130 meV at low temperatures. (iii) The excitation energy depends on the cross section of the nanowire. For the Sb nanowire annealed at 150 K, the excitation energy is 33 meV, 84 meV and 109 meV respectively for nanowires of diameters of 200 nm, 100 nm and 20 nm. The origin of such a variation of excitation energy is not known at present [48].

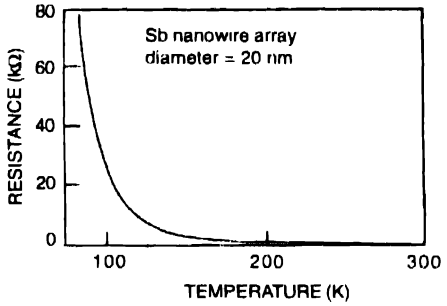

Figure 6. Schematic temperature dependence of the resistance of an Sb nanowire array with a diameter of 20 nm. This figure is based on the work of Barati and coworkers (Ref [48])

4.2.3. Semiconducting nanowires

Finally, we consider the behavior of resistivity of nanowires made of semiconducting materials. Zaitsev-Zotov and coworkers [36] have found that typical room temperature resistivity is more for the InSb nanowires ($L_x = 0.0 - 1.0$ mm, $L_y = L_z = 5 \pm 1$ nm) than for the bulk InSb by at least three orders of magnitude. They further found that a large number of InSb nanowires show a temperature dependence of resistivity of the form (Figure 7).

$$\rho \propto T^{-4}. \tag{15}$$

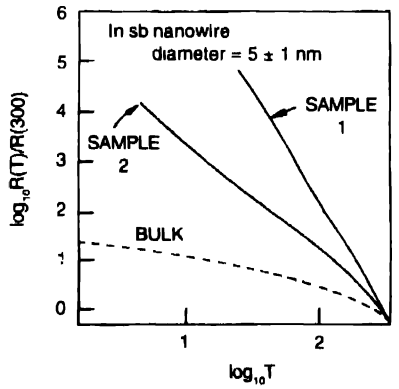

Figure 7. Schematic variation of linear conductance of InSb nanowires with temperature. This figure is based on the work of Zaitsev-Zotov and coworkers (Ref [36])

It is further seen that the I-V (I = current, V = potential) characteristics show a

$$I \propto V^b \qquad (2 \le b \le 6) \tag{16}$$

behaviour. This kind of power-like dependence of the current indicates that the electrons in InSb nanowires behave like a Luttinger liquid [89]. A brief description of the features of the Luttinger liquid is presented in Sec. 5.2.

Gu and coworkers [35] have synthesized Ge nanowires of diameters ranging from 20 nm to 180 nm, and have measured their resistivity. They have found that the resistance data of Ge nanowires is well described by the fluctuation-induced tunneling model [90], where the thermally activated voltage fluctuations across gaps are crucial in the determination of the temperature and electric field dependence of the conductivity. Empirically the resistance of the Ge nanowires is described by

$$R = R_0 \exp \frac{T_1}{T_1 + T_0} \tag{17}$$

Here, T_1 denotes the activation energy at high temperature and T_0 is a characteristic temperature.

4.2.4. Carbon nanotubes

We now consider the resistivity of the (n, n) single wall nanotubes (SWNTs). The resistance of the (n, n) SWNTs indicate a shallow minimum at a temperature $T = T^*$ [91] (Figure 8). The value of T^* is about 40 K, 180 K and 220 K for the single rope as grown mat and pressed mat respectively [91]. For $T > T^*$, the (n, n) SWNTs exhibit a positive slope in the resistance *versus* temperature curve, *i.e.* $d(\rho)/dT > 0$ (Figure 8). This is characteristic of a metallic behaviour. On the other hand, for $T < T^*$ the ρ vs T slope is negative, indicating a semiconducting feature [91]. Fischer and coworkers [91] attempted to explain their experimental observations by arguing that the diameters and resistances of SWNTs satisfy the Thouless criterion for 1D localization, thereby suggesting that weak localization may be responsible for the observed anomaly in the resistance. Kaiser and coworkers [92] gave another reason for the anomalous

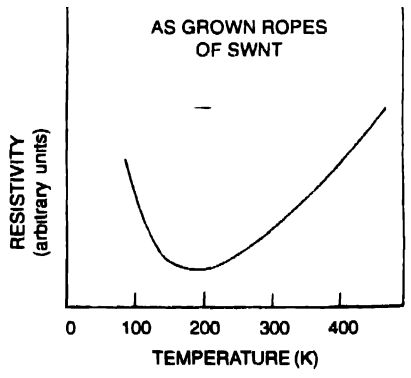

Figure 8. Schematic variation of resistivity of single-wall carbon nanotubes with temperature. This figure is based on the work of Fisher and coworkers (Ref. [91]).

behavior of the resistance of the SWNTs. They suggested that the observed anomaly in the behavior of ρ might be due to a possible mixing of metallic and disordered barrier regions that might have occurred during the formation of the SWNTs. Other suggested mechanisms consider the effect of intertube interaction within the bundle [93, 94] responsible for the observed behavior of the resistance. Yet another idea is based on the presence of both metallic and non-metallic nanotubes in the sample [93]. Kondo type effect has also been proposed for the explanation of the observed data [95]. Finally, Andriotis and co-workers [96] have given another explanation, which is based on the effects of residual transition metal catalycts (like Ni) residing in close contasts with the nanotube wall. There is therefore no unanimity in the mechanism responsible for the observed temperature variation of resistance of SWNTs.

4.3 *Coulomb drag*

Moving charges in a conductor exert a Coulomb force on the charge carriers in a nearby conductor and induce a drag current in the latter through a momentum transfer. This phenomenon, known as Coulomb drag, between spatially isolated, closely spaced electron systems has been the focus of considerable attention in the past few years [97-107], and experimental work on them was reported only recently [107, 108]. Experimental study of the drag resistance R_D with respect to variation of temperature, interwire distance, driving voltage and magnetic field shows that in the temperature region $0.2K \leq T \leq 1K$, R_D increases with decreasing temperature as $R_D \propto T^x$ where x ranges from -0.6 to -0.77 depending on the Fermi level position with respect to the 1D subbands. This feature of R_D cannot be understood on the basis of the Fermi liquid approach, and it is found that the Tomonaga-Luttinger liquid theory describes it much more successfully.

4.4 *Superconductivity*

In the bulk form many kind of materials show superconductivity below a critical temperature T_C [109-112]. The situation is expected to change when one starts to reduce the dimensions of superconducting system. In 1966 Mermin and Wagner [113] showed that it is impossible for the superconducting long-range order to survive in a strictly 1D system. This raises the question How and when does superconducting phase get extinguished as a bulk superconductor transits towards 1D form ? In 1967, Langer and Ambegaokar [114] and in 1970, McCumber and Halperin [115] proposed that below T_C one-dimensional superconductors have a finite resistance due to thermally activated phase slips. In 1972, Newbower, *et al* [116] verified this proposal by performing measurements on 0.5 μm diameter tin whiskers. However, Sharif, *et al* [117], performing measurements on homogeneous Pb wires, found that their data could not be explained by the LAMH (Langer, Ambegaokar, McCumber and Halperin) model [114, 115]. Subsequently, Giordano [118] performed measurements on thin In and PbIn wires. He found that from the LAMH (Langer, Ambegaokar, McCumber and Halperin) behaviour [114, 115] is valid only near T_C, and when the temperature is lowered, the resistance starts to follow a different behaviour. Giordano attributed this behaviour to phase slips occurring *via* macroscopic quantum tunneling, or quantum phase slips, through the same free energy barrier. Recently, Bezryadin, *et al* [59] have made experimental study of the superconducting behavior of Mo-Ge nanowires of diameters ≤ 10 nm, and length ~ 150 nm. The observation of these authors provide the following information :

(i) Samples of Mo-Ge nanowires with $R_N > R_q$ are superconducting while all samples with $R_N < R_q$ are insulating. Here, R_N is the normal-state resistance, and $R_q = h/4e^2 = 6.5$ kΩ is quantum resistance of Cooper pairs.

(ii) The superconducting as well as insulating properties become stronger when the difference $R_N - R_q$ increases in most of the cases.

(iii) The difference between the superconducting and insulating samples becomes more pronounced at lower temperatures, indicating that the transition is driven by quantum (not thermal) fluctuations.

The important role of the normal-state conductance $G_N = 1/R_N$, is evident from the measurements of Bezryadin, *et al* [59], and suggest that the observed superconductor-insulator transition is a *dissipative phase transition*, which is a sort of quantum localization transition [119-121].

Very recently, Lau and coworkers [122] measured temperature-dependent resistance of more than 20 superconducting nanowires of Mo-Ge with nominal widths ranging from 10 to 20 nm and lengths from 100 nm to 1 μm. They found that some of the superconducting samples having normal-state resistance R_N as high as 40 kΩ ($>> R_q$) are also superconducting. This means that the *dissipative phase transition* is not a relevant mechanism for controlling the superconductor-insulator transitions in Mo-Ge nanowires. Rather, the experimental data of Lau and coworkers suggest that the relevant parameter for the superconductor-insulator transition is resistance per unit length (R_N / L_x) or equivalently, the cross sectional area of the wire. In fact, the superconductor-insulator transition shown by the samples of Lau and coworkers includes both thermally activated phase slips close to T_C and quantum phase slips at low temperatures (below $T \sim T_C/2$)

4.5. *Optical behavior*

There have been lots of studies of the optical properties like photoluminescence [123, 124], polarized-light absorption [123, 125] and exciton binding energy [65] in nanowires in recent years. In photoluminescence, one irradiates the sample with a laser beam of fixed wavelength and then measures the emitted photoluminescent spectrum at different wavelengths. Lei and collaborators [124] have prepared TiO_2 nanowires of diameter less than 60 nm, and have made measurements of the

photoluminescence. They have found that the TiO_2 nanowire arrays show a spectrum in the visible range with three peaks, which are located at about 425, 465 and 525 nm. These peaks are attributed to self-trapped excitons, F centers and F^+ centers, respectively.

Alen and coworkers [123] have studied the photoluminescence and polarized-light absorption of several samples containing self-assembled InAs/InP quantum wires in the temperature range 30-300 K with an excitation wavelength of 514.5 nm and incident power density in the range 10^3– 10^4 W/cm^2. They have observed several resonances below the InP excitonic transition around 1.42 eV. On the basis of the observed results it has been argued that there is a strong intermixing in the hole subbands. The experimentally observed temperature dependence of the photoluminescence integrated intensity of the InAs/InP nanowires is accounted for by a model for excitonic recombinations, with two characteristic activation energies E_1 and E_2 [126].

$$I_{PL}(T) = \frac{I_0}{1+\tau_0\left[\Gamma_1 \exp\left(-E_1/k_BT\right)+\Gamma_2 \exp\left(-E_2/k_BT\right)\right]}. \tag{18}$$

Here, I_0 is the photoluminescence integrated intensity at $T = 0$ K, τ_0 is the radiative recombination time for exciton, and Γ_1 and Γ_2 are the two related scattering rates for the excitons.

4.6. Raman spectra

Zhang and coworkers [34] have measured Raman spectra of freestanding Ge nanowires for examining phonon confinement in these wires of diameter 20-51 nm. Raman spectroscopy shows shift in the peak position, broadening and asymmetry of the Raman bands in the Ge nanowires. Zhang and coworkers [34] have found no indication of the change of lattice parameter of the Ge core with stress. It appears that the profile and shape of the Raman peak may be attributed to the quantum confinement of optical phonons in the Ge nanowires. Because the nanowires in their experiments were long, thin and crystalline, there is a momentum $q = 0$ along the direction of the wire axis. However, in the direction perpendicular to the axis of the nanowires, the crystal size L_y, L_z is small, so that it corresponds to a large momentum $q = +2\pi / L_x, y$. Therefore, nonzero q phonon dispersion, which includes the optical phonons of Ge, may participate in Raman scattering and lead to both a peak broadening and an extension of the Raman peak towards low frequencies. Nanowires of very low diameters (6-17 nm) are found to show a tail also in the intensity *versus* Raman shift curve at low frequencies. The reason for this also appears to lie in the phonon confinement along the transverse direction [34].

4.7. Magnetic behavior

In 1994 Elmers and coworkers [127] found that submonolayer amounts of Fe on a W (110) surface with irregular atomic steps show ferromagnetism down to an Fe coverage of 0.05 ML. Smooth and coherent Fe stripes on W (110) still exhibited ferromagnetism at a coverage of 0.5 ML with an average monolayer stripe width of 20 atomic rows [128]. InAs/InP quantum wires having buried lattice mismatch have been studied by polarization analysis in high magnetic field upto 28 T [129]. The polarization anisotropy of 40 nm and 70 nm wires is not suppressed even at 28 T of magnetic field, and the Zeeman splitting becomes nonlinear. These abnormal features demonstrate that the strain of InAsP/InP nanowires is anisotropic triaxial and that symmetry of the strain is broken by the magnetic field [129]. There have been measurements of exchange interaction also of the Co nanowires by using angle-resolved photoemission spectroscopy with synchrotron radiation [28, 130]. The exchange interaction of the monatomic Co chain is found to be ~ 2.1 eV. This value is much higher than the typical values for thin Co films (2D systems) which is 1.4 – 1.9 eV, and for bulk (3D) Co material which is 1.4 eV. The enhancement of the exchange interaction is essentially a consequence of band narrowing due to the reduced atomic coordination in the 1D systems [28].

Other magnetic properties of nanowires are also quite different from the bulk samples. For example, ordered $Fe_{14}Ni_{86}$ alloy nanowire arrays embedded in an anodic alumnite template show an enhanced coercivity as high as 962 Oe and remnant magnetization up to 70% of the saturation magnetization [131]. The length and diameter of the $Fe_{14}Ni_{86}$ alloy nanowire used in the experiment were about 50 μm and 25-43 nm [131]. Such high coercivity material should be suitable for magnetic recording media, and, because the ideal storage density could reach about 200 G bit inch^{-2}, which is more than 2×10^5 times than that of 3.5 conventional floppy disc.

5. Theoretical understanding

Nanowires are, in general, quasi-1D systems, and are therefore expected to be qualitatively quite different from the thick (3D) wires and also from the ultrathin (1D) wires. For the 3D wires a successful description of the physics of electrons in the wire is given by the Fermi liquid approach. On the other hand, for the exactly 1D systems, a Luttinger liquid description is certainly a more appropriate description. Apart from the Luttinger liquid description, the Landauer approach is also used for the transport of electrons in 1D systems. In this section we provide a description of the main features of the Landauer approach and Luttinger liquid description. We shall also mention other theories, which are being used for discussing different physical properties of nanowires.

5.1. Landauer approach

A standard approach for calculating the scattering properties of nanowires is due to Landauer [132, 133]. The approach has been extremely useful not only as a tool to calculate conductance but also, perhaps more importantly, as a picture from which

physical insights on new phenomenon can be obtained. It is concerned with a given system, and no ensemble-averaging is necessary. Thus, mesoscopic fluctuation effects emerge very naturally. In 1957, Landauer [132] first introduced the 1D version, which consisted of a given barrier connected through ideal 1D wires (flat potentials) to some external source (*i.e.* a pair of electron reservoirs with different chemical potentials), which drives a current I through the 1D system. The barrier is characterized by its transmission coefficient $R = 1 - T$ (for linear transport and at zero temperature, we need T and R at the Fermi energy only). As emphasized by Landauer [133], it is very important to take the waves coming from the two reservoirs to be 'incoherent' with each other (*i.e.* having no definite phase relationship), otherwise nonphysical results follow for the time reversed situation. While we shall describe here Landauer approach for electrons, this approach is equally applicable to phonons [134].

5.1.1. *Conductance from current-voltage relationship*

Consider a conductor connected to two large contacts by leads as shown in Figure 9. The leads are assumed to be ballistic conductors, each having ν transverse modes. T is the average probability that an electron injected in lead 1 will transmit to lead 2. We assume that electrons can exit from the conductor into the contacts without any reflection (that is, the contacts are 'reflectionless'. The $+k_x$ states in lead 1 are occupied only by electrons coming in from the left contact and hence these states must have an electrochemical potential of μ_1. Similarly we can argue that the $-k_x$ states in lead 2 are occupied only by electrons coming in from the right contact hence must have an electrochemical potential of μ_2.

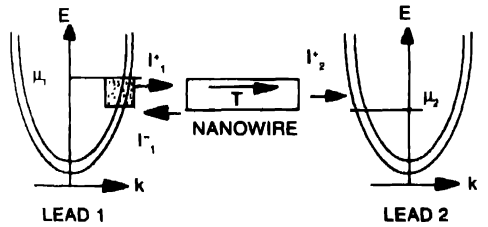

Figure 9. Schematic representation of the transmission process in the Landauer approach. The influx shown. T denotes the transmission probability through the nanowire.

Assuming zero temperature, current flow takes place entirely in the energy range between μ_1 and μ_2. The influx of electrons from lead 1 is given by

$$I_1^+ = (2e/h)\nu[\mu_1 - \mu_2]. \tag{19}$$

The outflux from lead 2 is simply the influx at lead 1 times the transmission probability T

$$I_2^+ = (2e/h)\nu T[\mu_1 - \mu_2]. \tag{20}$$

The rest of the flux is reflected back to lead 1, and is given by

$$I_1^- = (2e/h)\nu(1-T)[\mu_1 - \mu_2]. \tag{21}$$

The net current I flowing at any point in the device (and in the external circuit) is given by

$$I = I_1^+ - I_1^- = I_2^+ = (2e/h)\nu T[\mu_1 - \mu_2]. \tag{22}$$

Hence, the conductance is equal to

$$G = \frac{1}{(\mu_1 - \mu_2)/|e|} I_2^+ = \frac{2e^2}{h}\nu T. \tag{23}$$

In the ballistic regime, $T = 1$ and so eq. (10) is recovered from eq. (23).

5.1.2. *Conductance from Einstein relation*

In a later treatment [133], Landauer obtained the appropriate diffusion function and then invoked the Einstein relation to obtain the conductance. Consider electrons incident on an array of obstacles, and for conceptual clarification assume that there is a space free of obstacles at each end of the array. Let the reflection probability for the whole array be R. Then for a carrier incident from the left, the relative particle density in the free space to the left of the array will be $1 + R$ (after averaging over a space of several wavelengths), since both the incident and reflected stream are present. To the right of the obstacle, the density will be $1-R$; only the transmitted flux exists there. The density gradient across an array of length L will be grad $n = -2R/L$. The current, j, of particle associated with this gradient is $V(1-R)$ (V = electron velocity in the absence of scatterers). Using the diffusion equation, $j = -D$ grad n, this situation leads to a diffusion coefficient:

$$D = \frac{VL}{2}\left(\frac{1-R}{R}\right) \tag{24}$$

Any incoherent superposition of the 'from the left' and 'from the right' states will also be characterized by this same D. This is because 'from the right' will also give the same expression. An incoherent superposition can be presumed; coherence between waves emanating from the two independent 'black body' reservoirs at the two ends of the chain is not plausible. These reservoirs exert a phase randomizing influence on waves incident on them, and thus destroy phase memory before the particle can re-emerge from a black body into the obstacle array. Using eq. (24) and Einstein relation

$$\frac{1}{\rho}\,\frac{e^2 D}{\dfrac{\partial \mu}{\partial n}} \qquad \frac{e^2 VL}{2}\cdot\frac{1-R}{R} \Big/ \frac{\partial \mu}{\partial n} \tag{25}$$

in the form discussed by Kubo [135]. Landauer found that the conductance is given by

$$G = \frac{1-R}{2R} G_0 \tag{26}$$

In eq. (25), μ is the chemical potential corresponding to the density of n carriers.

5.1.3. Beyond Landauer approach

In 1986 Buttiker [136] extended the Landauer approach to the study of four-terminal phase coherent conductance. In particular, Buttiker proposed a Landauer formula that treats the current and voltage terminals in a four-period probe set up explicitly, and on an equal footing. The use of four-point probe is shown schematically in Figure 10. The Landauer theory and its modified version due to Buttiker are useful only for the processes where a DC field is applied. For the description of the processes connected with the AC field many formulation have been put forth. Kramer and Masek [24] have employed a quantum mechanical linear response theory where the influence of all scattering processes (elastic as well as inelastic) are treated on an equal (microscopic) footing. Their theory provides a framework for the identification of the transport channels in the Landauer theory. The quantum mechanical transmission probability amplitudes of the channel can be calculated microscopically. The other advantage of the theory of Kramer and Masek [24] is that it allows inclusion of the non-linear effects, which is not possible in the Landauer theory. Very recently, Safi [25] has developed a dynamic scattering approach for studying the AC field effects on the conductance of gated interacting wires.

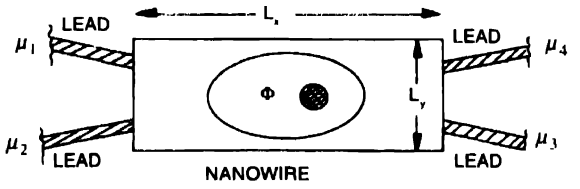

Figure 10. Disordered normal conductor (unshaded) with four terminals connected *via* perfect leads (shaded) to four reservoirs at chemical potentials μ_1, μ_2, μ_3 and μ_4. An Aharonov-Bohm flux Φ is applied through the hole of the sample.

5.2. Luttinger liquid approach

When the structure of the nanowire is such that its length is infinitely large ($L_x \to \infty$) and shows 1D behavior, it will be well described by the Luttinger liquid approach [89]. Such a situation is realized, for example, in the long InSb nanowires prepared by Zaitsev-Zatov and coworkers [36]. In those nanowires the carrier concentrations exceeds 10^{17} cm^{-3}. For an InSb nanowire of diameter 5 nm, the energy separation between the first and the second quantum levels is about 2×10^4 K, which far exceeds the room temperature. So, the electron band structure of 5 nm InSb wire is essentially one-dimensional and it shows a Luttinger liquid behavior [36]. It may, however be noted that Bi nanowire arrays of diameters 28 nm and 70 nm do not show Luttinger liquid behavior [137]. This is due to too large diameters of these Bi nanowires.

5.2.1. Density operator

A 'Luttinger liquid' involves two kinds of excitations left-moving electrons having energy

$$E_L = \left[\hbar v_F(-k - k_F)/2\pi\right] \tag{27}$$

and momentum $-k$. The right-moving electrons have energy

$$E_R = \left[\hbar v_F(k - k_F)/2\pi\right] \tag{28}$$

and momentum k. The left-moving and right-moving electrons may be combined to lead to another two types of 'excitations' - the 'charge' type excitations which correspond to the symmetric combination of the left-moving and right-moving electrons and the 'current' type excitations constructed from an antisymmetric combination of the left-moving and right-moving electrons.

In the case of 1D systems the electron energies and momenta have one-to-one correspondence. (The left-moving and right moving electrons are different entities). This is shown schematically in Figure 11. This is not true for the 2D and 3D systems where, for example, Fermi energy E_F corresponds to

Figure 11. Schematic representation of the domain of momenta of 1D systems which are occupied in the ground state between $[-k_F, k_F]$. Every point on this line corresponds to a single momentum and single energy, so that there is a one-to-one correspondence between energy and momentum. For a given energy transfer an electron of initial momentum k can make transition to the states k_1' and $k_2' = -k_1'$ for low energy transfer.

the numerous k points lying on the Fermi circle for 2D and on the Fermi sphere for 3D (Figure 12). The one-to-one correspondence of the electron energies and momenta in 1D allows characterization of the electrons in terms of bosons. Details of the bosonization process may be found, for example in Haldane [89]. Here we present qualitative features of the

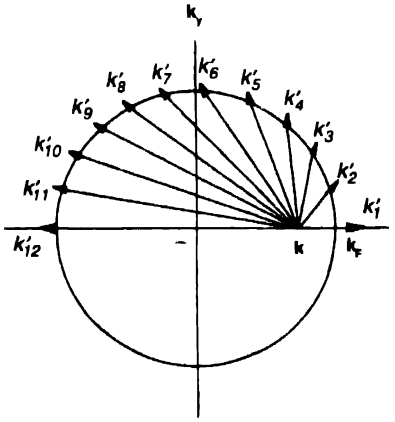

Figure 12. Schematic representation of the Fermi surface of 2D system which is a circle of radius k_F. While the energy on a given circle, which concentric to the Fermi circle is, same along the whole circumference different points of circumference will correspond to different momentum values. for a given energy transfer, an electron of initial momentum k can make transitions to the large number of momentum states some of which k_i'; i = 1, 2, 3...) are shown here by arrows.

bosonization process in a simplified way. Consider the creation and annihilation operators, $c^{+}_{L,-k}$ and $c_{L,-k}$ respectively, of a left moving electron of momentum k. (The creation and annihilation operators of a right-moving electron may be written similarly). In terms of $c^{+}_{L,-k}$ and $c_{L,-k}$, the density operator of the considered electron may be expressed as

$$\rho_{L,q} = \sum c^{+}_{L,-k+q} c_{L,-k} \qquad (q \neq 0) \tag{29}$$

and

$$\rho_{L0} = \sum c^{+}_{L,-k} c_{L,-k} - N_{L0} \quad (q = 0). \tag{30}$$

Here, N_{L0} is the number of the left-moving electrons in the ground state. The density operators of the left-moving electrons for different values of q do not commute. Rather, they satisfy the relation

$$\rho_{L,q}\rho_{L,q'} - \rho_{L,q'}\rho_{L,q} = -\delta_{q+q',0}(Lq/2\pi). \tag{31}$$

Here, $\delta_{q+q',0}$ is known as Kronecker delta function. In fact, $\delta_{q+q',0} = 1$ for $q + q' = 0$, while $\delta_{q+q',0} = 0$ for $q + q' \neq 0$.

5.2.2 *Bosonization*

The suggestion for bosonization arises from eqs. (29)-(31). It is different for $q > 0$ and $q < 0$, as is shown below :

$$a^{+}_{q} = (2\pi / L|q|)^{1/2} \rho_{R,q} \qquad (q > 0), \tag{32}$$

$$a_{q} = (2\pi / L|q|)^{1/2} \rho_{L,-q} \qquad (q > 0) \tag{33}$$

while

$$a^{+}_{q} = (2\pi / L|q|)^{1/2} \rho_{L,-q} \qquad (q < 0), \tag{34}$$

$$a_{q} = (2\pi / L|q|)^{1/2} \rho_{R,q} \qquad (q > 0). \tag{35}$$

The operator a^{+}_{q} and a_{q} are boson creation and annihilation operators, and correspond to energy $hv_F|q|/2\pi$ and momentum q. This is for the $q < 0$ or $q > 0$ modes. When consideration of the $q = 0$ mode is also made the net boson momentum will be $2k_F + \pi(N_L + N_R)/L$, where N_L (N_R) is the number of the left (right) moving electrons. A complete description of bosonization can be found in Haldane [89]. The advantage of bosonization is that in this process interaction terms become product of only two operators, which allow an easy calculation of properties of the system. The low energy properties of the model obtained after bosonization depend on five distinct parameters :

1. The Fermi field operator expressed by

$$\phi = (1/2)\tanh^{-1}\left(-V_{2q}/\left(v_F + V_{1q}\right)\right) \quad (q > 0). \tag{36}$$

2. The Fermi momentum k_F

3. The sound velocity

$$v_s = \left|\left(v_F + V_{1q}\right)^2 - \left(v_{2q}\right)^2\right|^{1/2} \quad (q \to 0). \tag{37}$$

4. The Fermi velocity

$$v_N = v_s e^{-2\phi} \tag{38}$$

associated with charge excitation, and

5. The Fermi velocity

$$v_J = v_s e^{2\phi} \tag{39}$$

associated with current excitations.

A key feature of the above treatment is that interaction appears in the power of the physical parameter *via* a function of $e^{-2\varphi}$ and/or $e^{2\varphi}$. For example, the I-V characteristics become non ohmic and are given by

$$I \approx V^{b}, \tag{40}$$

where

$$b = 2e^{-2\phi} - 1. \tag{41}$$

Notice that $b = 1$ corresponds to $\varphi = 0$. This means that if one obtains $b = 1$ in an experiment, then that case corresponds to noninteracting electrons. On the other hand, $b < 1$ ($b > 1$) corresponds to repulsive (attractive) interaction.

In must be emphasized that the "Luttinger liquid" behaviour as demonstrated by eq. (40) has no analogue in the 'Fermi liquid' behaviour. In fact, in the Fermi liquid behaviour I-V characteristics remain ohmic ; the effect of the interaction modifies only the resistance. Very recently, Rosch and Andrei [138] have employed the Luttinger liquid approach for studying the low temperature low-frequency conductivity of an interacting one-dimensional electron system in the presence of a periodic potential by including the umklapp scattering process.

5.2.3. *Effect of disorder*

Ogata and Fukuyama [83] have developed a Luttinger liquid approach for examining the effect of impurities in a nanowire. They have assumed that the carrier density n and nanowire width (L_y and L_z) are such we need only consider single subband of the nanowire. The electrons are supposed to be scattered by impurities and to interact mutually *via* long-range coulomb interaction. Electron- phonon interaction is neglected so that the study of Ogata and Fukuyama is valid only for low temperatures.

For the noninteracting electron case the conductance is found to be expressed by [83]

$$G = \frac{ne^2}{L_x m^*(-i\omega+\delta)} \qquad (\delta \to 0), \tag{42}$$

for $L_x \to \infty$, and by eq. (10) for finite L_x.

For the interacting electron case the conductance is given by

$$G = G_0 \eta / \left[1 + L_x F(T, L_x)/2v_F \tau_{tr}^0\right]. \tag{43}$$

Here, is already defined by eq. (11), v_F is Fermi velocity, $F(T, L_x)$ provides effect of impurity backward scattering at temperature T, and

$$\tau_{tr}^0 = \hbar / 2\pi D(0) n_i \left(u(2k_F)\right)^2 \tag{44}$$

is transport relaxation time for noninteracting electrons. In eq. (44), $D(0) = 1/2\pi h v_F$ is half of density -of-states per spin, n_i is impurity concentration, and $u(q)$ is the 1D Fourier transformation of random impurity potential for wave vector transform q.

5.2.4. *Break down of Luttinger liquid approach*

While a system of electrons interacting *via* a short-range interaction shows Luttinger liquid behaviour in one-dimension, it shows a Fermi liquid behaviour in two and three dimensions. Bellucci and Gonzalez [139] have examined the effect of long-range coulomb interaction on the one-dimensional systems. They have found that the Luttinger liquid behaviour is applicable only for dimensions $D = 1$. According to them, the proximity to the $D = 1$ fixed point strongly influences the phenomenology of quasi-one-dimensional systems, and that for any dimensions above $D = 1$ the interacting electron system follows marginal Fermi liquid behaviour.

5.3. *Other theoretical methods*

Apart from the theoretical methods described above which are suitable for very thin (1D) nanowires, there are other methods also for analyzing the physical behaviour of nanowires.

5.3.1. *Elasticity theory*

Goedecker and coworkers [140] have devised a method to determine the equilibrium geometry of large atomistic systems. Their method is based on a separate treatment of long and short wavelength components of the interatomic forces. The rapidly varying part of the forces has been handled by conventional methods, while the slowly varying part is treated by elasticity theory. Goedecker and coworkers have applied their method to a system containing up to 10^6 atoms, and argue that their linear scaling method is quite suitable for locating lower energy local minima.

5.3.2. *Molecular dynamics*

Barnett and Landman [141] have performed first-principles molecular dynamics simulations for Na nanowires. They show that the neck of the pulled wire is finally only a few atoms wide and that the atomic geometries at the neck can be derived from those of the isolated atomic clusters. Hermann and coworkers [142] have employed molecular dynamics using a density functional based tight-binding method for studying the problem of production of specific carbon nano structures. Their results show that it is possible to generate a large variety of carbon nanoparticles from precursors with known structures.

5.3.3. *Dynamic scattering approach*

Safi [25] has developed a dynamic scattering approach for gated interacting wire. He has encoded the perfect contact to charge reservoirs in time-dependent boundary conditions. The conductance matrix for an arbitrary gated wire, respecting charge conservation, is expressed through a dynamic scattering approach.

5.3.4. *Self-consistent field approach*

Moudgil [143] has used the self-consistent- field approximation of Singwi and coworkers [144] to investigate the possibility of finding a charge-density-wave instability in a zero-temperature double-quantum-wire structure. He has tested the intrawire and interwire correlations on an equal footing. The main result of Moudgil is that the double-quantum-wire structure may become unstable against a long-wavelength charge-density wave instability for sufficiently low electron density and nanowire width, in the close proximity of two wires.

5.3.5. *Transfer Hamiltonian approach*

Buldum *et al* [145] have used a model Hamiltonian approach to investigate the effects of the quantized nature of vibrational modes of a dielectric wire with thickness of atomic dimensions on phononic heat transfer between two reservoirs. Numerical calculations are performed for a model systems [146] for examining the heat transfer through a two atom chain placed between two reservoirs with large cross section. The main result of Buldum, *et al* is that the thermal conductance of a uniform atomic wire at low temperature is independent of material and increass linearly with temperature.

5.3.6. *Variational approach*

Bouhassoune and coworkers [65] have used a variational approach and the Lee-Low-Pines transformation [147] within the effective mass approximation to study the binding energy of an exciton in a cylindrical quantum well wire subject to an external magnetic field. They described the effect of quantum confinement by an infinitely deep potential well taking into consideration the interaction between the charge carriers (electrons and holes) and the optical phonons. The importance of polaronic corrections to the excitonic binding energy and the confinement introduced by a magnetic field are discussed.

3.7. Perturbation approach

reire and coworkers [148] have used perturbation technique or obtaining eigenvalues and eigenfunctions corresponding a Hamiltonian describing the magnetic wire structures. By ssuming that the spin degrees of freedom depend only on the enter of-mass coordinates of the exciton motion, they have nvestigated the exciton trapping in magnetic wire structures uch as $GaAs/Al_{0.3}Ga_{0.7}As$ systems.

3.8. s-d model

Krompiewski [67] has carried out numerical studies of onductances of ferromagnetic nanowires within the framework f 'semi-realistic' s-d model with the inter-atomic hybridization. He has developed a new approach by assuming that in the last tages of the breaking of the nanocontact, there are fewer and fewer conduction paths, distributed at random and stretching across the contact region. Conductance is calculated within the quasi ballistic regime, using the Kubo formula and a recursion Green's function technique. The main result of Krumpiewski is that conductances of weak ferromagnets and strong ferromagnets are qualitatively different. In fact, histograms corresponding to strong ferromagnets show small, densely distributed peaks, whereas, for a weak ferromagnet the peaks are clearly more pronounced.

3.9. Micromagnetic modeling

Hertel [149] has employed micromagnetic modeling wherein simulations are performed with an algorithm based on the finite element method which allows for the accurate calculations of magnetostatic interactions. This method is used for investigating the magnetic structures and magnetization processes in arrays of closely packed Ni nanowires (length $L_z = 1$ μm, diameter $L_x = L = 40$ nm and period = 100 nm). On the basis of his theoretical study Hertel [149] has found that magnetostatic interactions between the wires have a significant influence on the switching of the magnetic field.

3.10. Single-particle approach

Ihm and coworkers [150] have used the single-particle picture for studying the behaviour of a quantum wire with parabolic confinements in a longitudinal (along the x-direction) magnetic field Analytic solutions are obtianed for the eigenenergy spectrum and density of states. The effect of quantum confinements on the magnetization is seen to manifest in quantum oscillations, resulting in more profound structures than those found in the free electron case. The free electron case corresponds to three dimensional electron gas, where there is no confinement. At higher temperatures, however, the confinement effect is less visible and the magnetization reduces to the Landau diamagnetization of a free electron gas for $k_B T >> \hbar\omega$.

5.3.11. Jellium model

The jellium model has been employed to study metallic nanowires by a large number of workers [151-153]. Earlier studies show that the subband structure shown by nanowires is reflected as oscillations in the physical properties of the wire as its radius is varied [151-153]. In a later study of the jellium model, Zabala *et al* [154] predicted that a simple metal quantum wire, describable by jellium model, should show spontaneous magnetization for certain wire radii. In fact, in the case of jellium wires the perpendicular confinement causes the density of states to diverge near the bottom of each subband. If the highest occupied subband is just below the Fermi level the density of states at the Fermi level can attain high values resulting in a stable spin polarization of the jellium wire.

6. Concluding remarks

The study of nanowires is a rapidly developing field. It has opened many problems which require detailed experimental investigations as well as theoretical efforts for understanding them. There are interesting problems which need further investigations. Some of them are mentioned below :

(i) A study of nanowires of dimensions comparable to the electronic mean free path is needed because a complete picture is not there. There is lot of scope of further investigation in this area.

(ii) Most of the studies made upto now are based on the paramagnetic leads. What happens to the behavior of the nanowires when ferromagnetic leads are used in place of the paramagnetic ones. Such studies may be useful in developing magnetic devices.

(iii) There is a need for studying coupled wires. A detailed investigation will be helpful in gaining a clear picture for device development. It will be of interest to examine how the confinement fo electrons in coupled wires is reflected in the behavior of optical, magnetic, electric and other properties of the nanowires.

(iv) The Luttinger liquid approach provides a plausible explanation of the behavior of many types of nanowires. One problem that is interesting is to understand how long-range Coulomb interaction, backscattering and interference effects can modify the Luttinger liquid theory. Finally, it is also desirable to understand how a Luttinger liquid system behaves in the presence of disorder.

(v) It will also be interesting to study how the energy gap (excitation energy) depends on the cross sectional dimensions of the semiconducting nanowire.

(vi) The effect of disorder on the excitonic emission in strongly confined quantum systems in relation to its polarization anisotropy is an unsolved problem.

There is scope for both theoretical and experimental work here.

(vii) There is a need for searching for new superconducting nanowires. Metallic nanotube of NbS_2 is a candidate for becoming a superconductor. In fact, in the NbS_2 metallic nanotubes there is high density of states at Fermi energy. Moreoever, due to the tubule curvature the electron-phonon interaction is also expected to be significantly strong. Both of these effects suggest the possibility of superconductivity at higher critical temperatures for the NbS_2 tubes when compared to those reported for bulk NbS_2. The T_C of bulk NbS_2 is about 6.0 K.

(viii) Apart the above problems in electronic nanowires, there is a need for investigation of phonon nanowires. Measurements of phonon counting and double-slit interference experiments with single phonons are some problems the solution of which will sharpen our understanding about the physics of phonons in nanowires.

Acknowledgment

The authors are grateful to the Council of Scientific and Industrial Research for providing financial assistance vide scheme No. 70(0038)/00/EMR-II.

References

[1] T Ando *Nano-Physics and Bio-Electronics : A New Odyssey* eds T Chakraborty, F Peeters and U Sivan (Amsterdam : Elsevier) p1 (2002)

[2] Y Imry *Introduction to Mesoscopic Physics* (New York Oxford University Press) (1997)

[3] S Datta *Electronic Transport in Mesoscopic Systems* (Cambridge : Cambridge University Press) (1995)

[4] S Nahm, Y N Choi and S S Park *Appl Phys Lett* **80** 479 (2002)

[5] Y Huang, X Duan, Y Cui, L J Lauhon, K-Ha Kim and c M Lieber *Science* **294** 1313 (2001)

[6] S J Tans, R M Verschueren and C Dekker *Nature* **393** 49 (1998)

[7] R Martel, T Schmidt, H R Shea, T Hertel and Ph Avouris *Appl Phys. Lett.* **73** 2447 (1998)

[8] P G Collins, M S Arnold and Ph Avouris *Science* b292 **706** (2001)

[9] Z Yao, H W C Postma, L Balents and C Dekker *Nature* **402** 273 (1999)

[10] M S Fuhrer *Science* **288** 494 (2000)

[11] V Derycke, R Martel, J Appenzeller and Ph Avouris *Nano Letters* **1** 453 (2001)

[12] Y Cui, X Duan, J Hu and C M Lieber *J. Phys. Chem* **B 104** 5213 (2001)

[13] X Duan, Y Huang, Y Cui, J Whang and C M Lieber *Nature* **409** 66 (2001)

[14] Y Cui and C M Lieber *Science* **291** 851 (2001)

[15] D H Kim, S-K Sung, J S Sim, K R Kim, J D Lee, B-G Park, B H Choi, S W Hwang and D Ahn *Appl. Phys. Lett.* **79** 3812 (2001)

[16] Y Takahashi, M Nagase, H Namatsu, K Kurihara, K Iwadate, Y Nakajima, S Horiguchi, K Murase and M Tabe *Electron Lett* **31** 136 (1995)

[17] K Uchida, J Koga, R Ohba and A Toriuni *Tech. Dig.-Int Electron Devices Meet.* 863 (2000)

[18] Y Ono, Y Takahashi, K Yamazaki, M Nagase, H Namatsu, K Kurihara and K Murase *Appl. Phys. Lett.* **76** 3121 (2000)

[19] Y Takahashi, A Fujiware, K Yamazaki, H Namatsu, K Kurihara and K Murase *Appl. Phys. Lett.* **76** 637 (2000)

[20] A Rudra, R Hondre, J F Carlin and M Ilegems *J. Cryst Growth* **136** 278 (1994)

[21] A Ponchet, A Le Corre, H L Haridon, B Lambert and S Salun *Appl Phys. Lett.* **67** 1850 (1995)

[22] J Brault, M Gendry, G Grenet, G Hollinger, Y Desieres and T Benyatton *Appl. Phys. Lett.* **73** 2932 (1998)

[23] L Gonzalez, J M Garcia, R Garcia, F Briones, J M-Pastor and C Ballesteros *Appl. Phys Lett.* **76** 1104 (2000)

[24] B Kramer and J Masek *quantum Fluctuations in Mesoscopic and Macroscopic Systems* (Singapore : World Scientific) p3 (1991)

[25] I Safi *Euro Phys. J. B* **12** 451 (1999)

[26] C L Kane and M P A Fischer *Phys. Rev* **B46** 15233 (1992)

[27] A I Yanson, I K Yanson and J M Van Ruitenbeek *Phys Rev Lett* **84** 5832 (2000)

[28] A Dallmeyer, C Carbone, W Eberhardt, C Pampuch, O Rader W Gudat, P Gambardella and K Kern *Phys. Rev* **B61** R 5133 (2000)

[29] C Durkan and M E Welland *Phys Rev* **B61** 14215 (2000)

[30] O Gulseren, F Ercolessi and E Tosatti *Phys Rev Lett* **80** 3775 (1998)

[31] O Gulseren, F Ercolessi and E Tosatti *Phys Rev* **B 51** 7377 (1995)

[32] B Wang, S Yin, G Wang and J Zhao *J. Phys Condens Matter* **13** L403 (2001)

[33] U Landman, R N Barnett, A G Scherbakov and P Avouris *Phys Rev. Lett* **85** 1958 (2000)

[34] Y F Zhang, Y H Tang, N Wang, C S Lee, I Bello and S T Lee *Phys Rev.* **B 61** 4518 (2000)

[35] G Gu, M Burghard, G T Kim, G S Dusberg, P M Chiu, V Krstic and S Roth *J Appl. Phys.* **90** 5747 (2001)

[36] S V Zaitsev-Zotov, Y A Kumzerov, Y A Firsov and P Monceau *J Phys. : Condens Matter* **12** L303 (2000)

[37] A M Morales and C M Lieber *Science* **279** 208 (1998)

[38] Y F Zhang, Y H Tang, N Wang, D P Yu, C S Lee, I Bello and S T Lee *Appl Phys. Lett* **72** 1835 (1998)

[39] Y H Tang, Y F Zhang, C S Lee, N Wang, D P Yu, I Bello and S T Lee *Mater. Res. Soc Symp. Proc.* **526** 73 (1998)

[40] H Dai, E W Wang, Y Z Lu, S Fau and C M Lieber *Nature* (London) **375** 769 (1995)

[41] Y Zhang, K Suenaga, C Colliex and S Iijima *Nature* (London) **281** 973 (1998)

[42] X T Zhou, N Wang, H L Lai, H Y Peng, I Bello, N B Wong C S Lee and S T Lee *Appl. Phys. Lett.* **74** 392 (1999)

[43] w Q Hau, S S Fau, Q Q Li and Y D Hu *Science* **277** 1287 (1997)

[44] Y H Tang, X Y Sun, F C K Au, L S Liao, H Y Peng, C S Lee, S T Lee and T K Sham *appl. Phys. Lett.* **79** 1673 (2001)

[45] Y Zhang *Solid State Commun.* **115** 51 (2000)

[46] X F Wang, J Zhang, H Z Shi, Y W Wang, g W Meng, X S Peng, L D Zhang and J Fang *J. Appl. Phys.* **89** 3847 (2001)

[47] Yu-Ming Lin, S B Cronin, O Rabin, J Y Ying and M S Dresselhaus **79** 677 (2001)

[48] M Barati, J C L Chow, P K Ummat and W R Datars *J. Phys : Condens. Matter* **13** 2995 (2001)

[49] K tanaka, S Iwama and K Mihama *Japan J. Appl. Phys.* **37** L 669 (1998)

[50] D goldberg, Y Bando, K Kurashima and T Sato *Solid State Commun.* **116** 1 (2000)

[51] C N R Rao, B C Satish Kumar, A Govindraj and M Nath *Chem. Phys. Chem.* **2** 78 (2001)

[52] M Nath, A Govindraj and C N R Rao *J. Am. Chem. Soc.* **123** 4841 (2001)

[53] M H Whangbo and H J Koo *Solid State Commun.* **115** 675 (2000)

[54] P Millet *Solid State Chem.* **147** 676 (1999)

[55] F X Zha, R Czrew, D L Caroll, Ph. Redlich, B-Q Wei, A Loiseau and S Roth *Phys. Rev.* **B4884** (2000)

[56] S Ijima *Nature* **361** 333 (1994)

[57] W Han, Ph Redlich, F Ernst, M Ruhle *Appl Phys. Lett* **76** 652 (2000)

[58] W Q Han *Solid State Commun* **115** 527 (2000)

[59] A Bezryadin, C N Lau and M Tinkham *Nature* **404** 971 (2000)

[60] H Omi and T Ogino *Appl Phys Lett* **71** 2163 (1997)

[61] H Namatsu, M Nagase, K Kurihara, K Iwadate, T Furuta and M Murase *J Vac. Sci Technol* **B13** 1473 (1995)

[62] N Kramer, H Birk, J Jorritsma and C Schoenberger *Appl Phys Lett* **66** 1325 (1995)

[63] B Kramer and J Masek *J. Phys. C : Solid State Commun* **101** 149 (1997)

[64] T Sugaya, J P Bird, M Ogura, Y Sugiyama, D K Ferry and K Y Jang *Appl Phys. Lett* **80** 434 (2002)

[65] M Bouhassoune, R Charroui, M Fliyou, D Bria and A Nougaoui *J Appl Phys* **91** 232 (2002)

[66] T Suguya, M Ogura, Y Sugiyama, T Shimizu, K Yonai, K Y Jang, J P Bird and D K Ferry *Appl Phys Lett.* **79** 371 (2001)

[67] S Krompiewski *J Phys. : Condens. Matter* **12** 1323 (2000)

[68] B J van Wees, H van Houten, C J W Beenakker, J G Williamson, L P Kouvenhoven, D van der Morel and C T Foxon *Phys. Rev Lett* **60** 848 (1988)

[69] D A Wharam, T J Thornton, R Newbury, M Pepper, H Ahmed, J E F Forst, D G Hasko, D C Peacock, D A Ritchie and G A C Jones *J Phys C Solid State Phys.* **21** L209 (1988)

[70] F Ott, S barberan, J G Lunney, J M D Coey, P Berthet, A M Leon-Guevara and A Revcolevschi *Phys. Rev.* **B 58** 4656 (1988)

[71] J L Costa-Kramer *Phys Rev* **B 55** R4875 (1997)

[72] N Hamada, S Sawada and A Oshiyama *Phys. Rev. Lett* **68** 1579 (1992)

[73] J W Mintmire, B I Dunlap and C T White *Phys. Rev. Lett* **68** 631 (1992)

[74] R Saito, M Fujita, G Dresselhaus and M S Dresselhaus *Appl Phys. Lett* **60** 2204 (1992)

[75] H J Choi, J Ihm, S G Louie and M L Cohen *Phys Rev. Lett* **84** 2917 (2000)

[76] K J Thomas, J T Nisholls, N J Appleyard, M Y Simmons, M Pepper, D R Mace, W R Tribe and D A Ritchie *Phys Rev* **B 58** 4846 (1998)

[77] K J Thomas, J T Nicholls, M Y Simmons, M Pepper, D Mace and D A ritchie *Phys. Rev. Lett.* **77** 135 (1996)

[78] G Fasol and H Sakaki *Jpn. J. Appl. Phys.* **33** 879 (1994)

[79] D L Maslov *Phys. Rev.* **B 52** R14368 (1995)

[80] T Rejec, A Ramsak and J H Jefferson Preprint cond-mat/99 10399 (1999)

[81] T Rejec, A Ramsak and J H Jefferson *J. Phys. : Condens Matter* **12** L233 (2000)

[82] S Tarucha, T Honda and T Saku *Solid State Commun* **94** 413 (1995)

[83] M Ogata and H Fukuyama *Phys. Rev Lett* **73** 468 (1994)

[84] D L Maslov and M Stone *Phys Rev.* **B 52** 5539 (1995)

[85] K Schwab, E A Hnriksen, J M Worlook and M L Roukes *Nature* **404** 974 (2000)

[86] L G C Rego and G Kirczenow *Phys Rev Lett* **81** 232 (1998)

[87] A F Mayadas, M Shatzkes and M Janak *Appl Phys Lett* **14** 345 (1969)

[88] A F Mayadas and M Shatzkes *Phys Rev* **B1** 1382 (1970)

[89] F D M Haldane *J Phys C : Solid State Phys* **14** 2585 (1981)

[90] P Sheng *Phys Rev* **B 21** 2180 (1980)

[91] J E Fischer, H Dai, A Thess, R Lee, N M Hanjani, D L Dehaas and R E Smalley *Phys. Rev* **B 55** R4921 (1997)

[92] A B Keiser, G Dusberg and S Roth *Phys Rev* **B 57** 1418 (1998)

[93] J Hone, I Ellwood, M Muno, A Mizel, M L Cohen, A G Rinzler, R E Smalley *Phys Rev Lett* **80** 1042 (1998)

[94] P Delaney, H J Choi, J Ihm, S G Louie and M L Cohen *Nature (London)* **391** 466 (1998)

[95] L Grigorian, G U Sumaraseckera, A L Loper, S L Fang, J L Allen and P C Eklund *Phys Rev* **B 60** R11309 (1999)

[96] A N Andriotis, M Menon and G E Froudakis *Phys Rev* **B 61** 13393 (2000)

[97] Yu M Sirenk and P Vasilopoulos *Phys Rev* **B 46** 1611 (1992)

[98] Y-K B Hu and K Flensberg *Hot Carriers in Semiconductors* eds K Hess (New York Plenum) p261 (1996)

[99] B Tanatar *Phys. Rev* **B 58** 1154 (1998)

[100] V L Gurevich, V B Penzner and E W Fenton *J Phys Condens. Matter* **10** 2551 (1998)

[101] O E Raichev and P Vasiloqoulos *Phys Rev* **B 61** 7511 (2000)

[102] J Voit *Rep Prog Phys* **57** 977 (1994)

[103] F Flensberg *Phys Rev Lett* **81** 184 (1988)

[104] Yu A Nazarov and D V Averin *Phys Rev Lett.* **81** 653 (1998)

[105] R Klesse and A Sterne *Phys. Rev* **B 62** 16912 (2001)

[106] V V Ponomarenkov and D V Averin *Phys Rev Lett* **85** (2001)

[107] P Debray, V Zverev, O Raichev, R Klesse, P Vasilopoulos and R S Newrock *J Phys : Condens. Matter* **13** 3389 (2001)

[108] P Debray, P Vasilopoules, D Raichev, R Perrin, M Rehman and W C Mitchel *Physica* **E 6** 694 (2000)

[109] M Tinkham *Introduction to Superconductivity* (New York : McGraw-Hill) (1996)

[110] R Lal and S K Joshi *Phys Rev* **B 41** 1894 (1990)

[111] R Lal and S K Joshi *Phys Rev* **B 45** 361 (1992)

[112] T Ishiguro and K Yamaji *Organic Superconductor* (Berlin : Springer-Verlag) (1990)

[113] N D Mermin and H Wagner *Phys. Rev. Lett.* **17** 1133 (1966)

[114] L S Langer and V Ambegaokar *Phys. Rev* **164** 498 (1967)

[115] D E McCumber and B I Halperin *Phys Rev* **B1** 1054 (1970)

[116] R S Newbower, M R Beasley and M Tinkham *Phys. Rev.* **B5** 864 (1972)

[117] F Sharifi, A V Herzog and R C Dynes *Phys. Rev. Lett.* **71** 428 (1993)

[118] N Giordano *Physica* **203B** 460 (1994)

[119] G Schon and A D Zaikin *Phys Rep* **198** 237 (1990)

[120] S A Bulgadaev *JETP Lett.* **39** 315 (1984)

[121] A Schmid *Phys. Rev. Lett.* **51** 1506 (1983)

[122] C N Lau, N Markovic, M Bockrath, A Bezryadin and M Tinkham *Phys Rev Lett.* **87** 217003 (2001)

[123] B Alen, J M-Pastor, A G-cristobal, L Gonzalez and J M Garcia *Appl Phys Lett.* **78** 4025 (2001)

[124] Lei, L D Zhang, G W Meng, G H Li, X Y Zhang, C H Liang, W Chen and S X Wang *Appl Phys Lett* **78** 1125 (2001)

[125] R Kamalakaran, A K Singh and O N Srivastava *J Phys Condens. Matter* **23** 2681(2000)

[126] E M Daly, T J Glynn, J D Lambkin, L Considine and S Walsh *Phys Rev* **B52** 4696 (1995)

[127] H J Elmers *et al Phys Rev Lett* **73** 898 (1994)

[128] J Hauschild, H J Elmers and U Gradmann *Phys Rev.* **B 57** R677 (1998)

[129] M Notomi, J Hammersberg, J zeman, H Weman, M Potemski, H Sugiura and t Tamamura *Phys Rev Lett* **80** 3125 (1998)

[130] K Kern *Nature* **416** 300 (2002)

[131] H Zhu, S Yang, G Ni, S Tang and Y Du *L Phys. Condens. Matter* **13** 1727 (2001)

[132] R Landauer *I B M J Res Dev* **1** 223 (1957)

[133] R Landauer *Phil Mag* **21** 863 (1970)

[134] Y Imry and R Landauer *Rev Mod Phys* **71** S306 (1999)

[135] R Kubo *J Phys Soc. Jpn* **12** 570 (1957)

[136] M Buttiker *Phys Rev Lett* **57** 1761 (1986)

[137] J Heremans, C M Trush, Z Zhang, X Sun, S M Dresselhaus, Y J Ying and D T Morelli *Phys. Rev.* **B 58** R10091 (1998)

[138] A Rosch and N Andrei *Phys. Rev. Lett.* **85** 1092 (2000)

[139] S Bellucci and J Gonzalez *Phys. Rev* **B 64** R 201106 (2001)

[140] S Goedecker, F Lancon and T Deutsch *Phys. Rev.* **B 64** R161102 (2001)

[141] R N Barnett and U Landman *Nature* (London) **387** 788 (1997)

[142] H Hermann, F Fugacin and G Seifert *Appl. Phys Lett* **79** 63 (2001)

[143] R K Moudgil *J. Phys ; Condens. Matter* **12** 1781 (2000)

[144] K S Singwi, M P Tosi, R H Land and A Sjolauder *Phys Rev* **176** 589 (1968)

[145] A Buldum, S Giraci and C Y Fong *J. Phys : Condens Matter* **12** 3349 (2000)

[146] A Buldum PhD Thesis (Bilknet University, Turkey) (1992)

[147] T D Lee, F Low and D Pines *Phys. Rev* **90** 297 (1953)

[148] J A K Freire, F M Peeters, V N Freire and G A Farias *J Phys Condens. Matter* **13** 3283 (2001)

[149] R Hertel *J. Appl Phys* **90** 5752 (2001)

[150] G Ihm, M L Falk S K Noh, S J Lee and T W Kim *Phys Rev* **B 46** 15270 (1992)

[151] C A Stafford, D Baeriswyl and J Burki *Phys Rev Lett* **79** 2863 (1997)

[152] J M van Rutinbeck, M H Devoret, D Esteve and C Urbina *Phys Rev* **B 56** 12 566 (1997)

[153] C Yannouless and U Landman *J Phys Chem* **B 101** 5780 (1997)

[154] H Zabala, M J Puska and R M Nieminen *Phys Rev Lett* **80** 3336 (1998)